OXIDATION/CORROSION IN MATERIALS FOR SUPERCRITICAL CO_2 POWER CYCLES

S. C. Kung,[1] J. P. Shingledecker,[1*] D. Thimsen,[1] I. G. Wright,[2] B. M. Tossey,[3] and A. S. Sabau[4]

1 – Electric Power Research Institute, Charlotte, NC USA
2 – WrightHT, Denver, CO USA
3 – DNV-GL, Dublin, OH USA
4 – Oak Ridge National Laboratory, Oak Ridge, TN USA

Dr. John Shingledecker is a Program Manager in the Materials & Chemistry research area of the Electric Power Research Institute (EPRI). He is the leader of EPRI's Program 87, Fossil Materials and Repair, which provides the power industry with material use and selection guidelines, welding and repair solutions, corrosion mitigation methodology, and remaining life tools to increase plant availability, reduce failures, and improve efficiency. He has published more than 100 papers and reports on the metallurgy and behavior of high-temperature engineering alloys.

*Corresponding Author: jshingledecker@epri.com

ABSTRACT

Supercritical CO_2 (sCO_2) Brayton cycles are being considered for future fossil energy systems. These sCO_2 systems offer the possibility of improved efficiency combined with smaller turbo-machinery size compared to a traditional Rankine steam system if operated at turbine inlet temperatures up to 760°C. The overall objective of this cross-cutting materials project is to provide computational predictions of the oxidation performance (particularly the propensity for scale loss and associated small passage blockage) of structural alloys in supercritical CO_2 under severe operating environments at high temperatures. As part of this work, a laboratory study is being performed to generate the corrosion data needed for the design and construction of key components. This paper addresses two short-term laboratory tests, which exposed three commercial alloys to simulated sCO_2 working fluid with and without the addition of impurities at 700°C and 200 bar for 300 hours expected in future transformational fossil power cycles. A thick oxide scale formed on ferritic steel Gr 91 while the scales formed on austenitic stainless steel 304H and nickel-based alloy 740H were thin. In comparison, the weight gains of all three alloys were greater in pure sCO_2 than those containing 3.6% O_2 and 5.3% H_2O as impurities. In addition, the scale morphology formed on Gr 91 in pure sCO_2 appears to contain an intermediate oxide layer between the magnetite and spinel layers typically observed in high-temperature steam. Micro-hardness measurements were performed to determine the extent of carburization attack in the alloys from the sCO_2 exposures. Gr 91 suffered severe carburization from pure sCO_2, with a carburization depth up to 200 µm after only 300 hours. Less carburization was observed in Gr 91 when exposed to impure sCO_2 containing O_2 and H_2O presumably due to the higher partial pressure of oxygen and thus the formation of a more protective oxide scale. Carburization was also found in 304H after 300-hour exposure to sCO_2.

On the other hand, no carburization was observed in 740H. The superior carburization resistance of 740H was likely achieved by its higher Cr and Ni contents.

INTRODUCTION

Supercritical CO_2 (sCO_2) Brayton cycle operating at temperatures greater than 600°C offers the potential to significantly improve plant efficiency for future electric power generation. However, limited data are available on the oxidation and carburization behaviors of structural alloys exposed to sCO_2 at these temperatures. Most of the existing data are reported in terms of weight gain which does not allow for direct assessment of scale growth (thickness) kinetics which are important when considering the potential for exfoliation of oxides scales. The lack of suitable corrosion data severely hinders materials selection for the design and construction of high-temperature components of these advanced cycles, such as heaters and recuperators. It is generally assumed that the oxidation kinetics and scale formation for alloys exposed to sCO_2 are similar to those under high-temperature high-pressure steam conditions. However, compared to steam, the consumption of oxygen from sCO_2 oxidation could promote carburization of alloys, especially where the oxygen potential is relatively low. As a result, the oxidation and corrosion mechanisms operating on alloys under sCO_2 may be different from those under high-temperature steam. Such differences, if they exist, must be well understood before materials of construction can be adequately selected for the advanced sCO_2 cycles.

A laboratory study is being performed by EPRI and its collaborators as part of the effort to generate the corrosion data needed for the design and construction of key components in advanced sCO_2 Brayton power cycles. The objective of this study is to generate corrosion information directly useful for the selection of alloys exposed to high-temperature and high-pressure sCO_2 environments. Exposures for short-term tests were conducted for 300 hours on a limited group of alloys to validate the approach and select the long-term test conditions. Longer-term tests, now started, are aimed to last for 1000 to 5000 hours. Following the laboratory testing, the process of oxide growth and exfoliation on alloy surfaces, with and without carburization, will be modeled under realistic, non-isothermal conditions (i.e., with heat-flux) for geometries expected in compact heat-exchanger surfaces and used to predict long-term component performance.

Discussion of the results of the laboratory testing is the focus of this paper. At the time of the paper writing, two short-term tests have been completed, while the long-term tests and modeling work were still ongoing. Therefore, only the short-term test results are presented here, and the remaining laboratory and modeling work will be the subject of a separate publication in the future.

CALCULATIONS OF sCO_2 OPERATING CONDITIONS

Relatively pure sCO_2 working fluid is anticipated for indirect-fired closed sCO_2 Brayton cycles. However, the sCO_2 working fluid of direct oxy/natural gas-fired open Brayton power

cycles is expected to contain a number of contaminants, as impurities in the fuel and oxygen streams are introduced to the combustion. These contaminants will flow through the combustor, turbine and low-pressure side of the power cycle. Some of the contaminants can be actively removed prior to CO_2 re-compression, but the concentrations of certain species will increase in the gas stream before combining with the CO_2 produced from combustion of the carbonaceous fuel. The major contaminants in oxy/natural gas-fired sCO_2 based on evaluation of ref [1,2] are:

- H_2O - Water vapor is produced during combustion of hydrocarbon fuels. This contaminant will be largely removed from the circulating sCO_2 by condensation in the compressor inlet cooler/condenser. The working fluid will enter the compressor saturated with water at the temperature leaving the cooler/condenser.
- O_2 – Some level of excess oxygen will be required for complete combustion. Oxygen will leave the circulation loop only in the bleed CO_2 stream.
- N_2 – Nitrogen will enter the loop as traces in both the fuel gas stream and the oxygen stream. Small amounts of the N_2 will be converted to NO_x in the flame. Nitrogen will leave the circulation loop only in the bleed CO_2 stream.
- Ar – Argon will enter the loop as a trace in the oxygen stream. Argon will leave the circulation loop only in the bleed CO_2 stream.
- NO_x – Very small amounts of NO_x will be produced in the flame. If the lead chamber process[2] is employed on the low-pressure working fluid stream, which treats the contaminated working fluid upstream of the inlet cooler/condenser, essentially all of the NO_x produced will be converted to nitric acid and removed by the aqueous condensate collected in the compressor inlet cooler/condenser. Otherwise, the NO_x will leave the circulation loop only in the bleed CO_2 stream.
- SO_x – Any sulfur entering with the fuel will be converted to SO_2/SO_3 in the flame. If the lead chamber process[2] is employed on the low-pressure working fluid stream, nearly all of the SO_2 in the working fluid will be converted to SO_3 and removed as sulfuric acid in the aqueous condensate collected in the compressor inlet cooler/condenser. Otherwise, the SO_2 will leave the circulation loop only in the bleed CO_2 stream.
- HCl – Chloride in the fuel gas will be converted to hydrogen chloride in the flame. The HCl will be removed into the aqueous condensate collected at the compressor inlet cooler/condenser.

An estimate of the contaminant levels was made for a prototype open Allam cycle.[1] The recycle sCO_2 flow is approximately 35 times the molar flow of methane. Using this ratio adjusted for a constant LHV input to the cycle, a simple mass balance was performed to estimate the working fluid contaminant levels for two fueling scenarios:

1. Methane fueling – This is the cleanest case and represents the lower limit of contaminants that might be expected in the working fluid.
2. Cooled, raw coal syngas-fueling – This is the case that gives upper limits to HCl and SO_x in the working fluid. This approach is taken in the expectation that overall efficiency

would be maximized by removing SO_x and NO_x from the Brayton cycle working fluid rather than in the coal gasification island. As mentioned, a reactor employing the lead chamber process treats the contaminated working fluid upstream of the inlet cooler/condenser.[2] In this process, SO_x in the working fluid upstream of the inlet cooler/condenser is converted to H_2SO_4 and NO_x is converted to HNO_3. These acids are highly soluble in water and can dissolve in the condensate collected by the compressor inlet cooler/condenser.

The fuel used for the coal syngas case was based on a model composition developed from data previously published by USDOE[3] for gasification of a 2.7wt% sulfur, 0.3wt% chlorine (coal basis) Illinois bituminous coal and is indicated in Table 1 as is a model composition for merchant oxygen. The resulting working fluid composition for the two cases is given in Table 2. For each fuel case, two working fluid compositions are shown: (1) the recirculating sCO_2 at the combustor inlet and (2) the products of combustion entering the gas turbine.

Table 1
Composition of model fuels and model oxidant

Species	Composition (mol%)		
	Methane	Cooled raw coal syngas	Oxygen
CH_4	100	1.0	
CO		39.0	
H2		28.3	
CO_2		8.0	
H_2O		20.0	
N_2+Ar		2.0	0.5
H2S		0.9	
HCl		0.02	
O_2			99.5
LHV	912 BTU/scf	218 BTU/scf	

Table 2
Estimated Working Fluid Composition

Component	Composition (mol% or mol ppm)			
Fuel	Methane		Cooled Raw Coal Syngas	
Stream	Combustor Inlet	Turbine Inlet	Combustor inlet	Turbine Inlet
CO_2	95	90	90	85
H_2O	250 ppm	5	250 ppm	5
N_2+Ar	1	1	9	9
O_2	4	4	1	1
HCl				20 ppm
SO_2				1000 ppm

Notes:

- *The higher concentration of N_2+Ar in the coal syngas-fueled case is caused by the elevated nitrogen content of the syngas.*
- *The reduced oxygen content for the coal syngas-fueled case is largely explained by higher CO_2 bleed rates due to the elevated CO_2 content of the fuel gas. A secondary effect is the reduced oxygen required (per unit LHV) to burn syngas compared to methane.*
- *H_2O concentrations at the combustor inlet were calculated to be those associated with saturated gas at 38°C (100°F) and 275 bar (4000 psia) total gas pressure.*
- *There are no reliable reports of excess oxygen required to avoid carbon monoxide in the products of combustion at the very high combustor pressures associated with the Allam cycle. The calculation performed assumed 2% excess oxygen feed to the combustor. Oxygen concentrations in the working fluid can rise and fall with the excess oxygen required.*
- *There are no reliable reports of NO_x production at the high pressures associated with the direct-fired Brayton power cycle. The NO_x levels would likely be low due to the comparatively low firing temperatures anticipated (1150°C) and the low nitrogen concentrations (compared to air-firing in combustion turbines).*

To further validate the gas compositions in Table 2 derived from simple mass balance, detailed thermodynamic calculations were performed using a commercial software, *HSC Chemistry 8*.[4] In the thermodynamic treatments, both mass balance and Gibbs energy minimization were considered simultaneously. Therefore, chemical species were redistributed through chemical reactions to allow the system to reach the lowest Gibbs energy state (i.e., equilibrium). Such redistribution is especially important for corrosive species of interest, which are typically minor in concentration and cannot be estimated by using mass balance alone. In these thermodynamic treatments, the same fuel compositions for methane and syngas shown in Table 1 were used, and the calculations were carried out with 2vol% excess O_2 in the combustion gas at 700°C and 200 bar.

Results of the thermodynamic calculations, summarized in Table 3, shows the concentrations of the selected species of interest present in the combustor prior to dilution by the recycled CO_2. Noticeably, the concentration of CO_2 from the syngas is much higher than that of methane, while the moisture content from the syngas is significantly lower than that of methane. Such differences are attributed to the high hydrogen content of methane (as CH_4). From the standpoint of high-temperature corrosion, the combustion gas from syngas contains much higher concentrations (vol) of HCl and SO_2 (969 ppm and 8500 ppm, respectively) than those from methane (0 and 1 ppm, respectively).

Table 3
Equilibrium concentrations of selected species produced from the combustor of O_2-fired sCO_2 Allam cycle (in mol%=vol%)

Species	Methane	Syngas
CO_2	33.8	62.9
HCl	nil	0.0969
H_2O	65.6	33.7
O_2	1.31	1.48
N_2+Ar	0.33	0.9
NOx	nil	0.0025
SO_2	0.0001	0.85

Once the combustion gas is diluted with recycled CO_2 that has been scrubbed by a condenser upstream, the concentrations of HCl and SO_2, as well as the moisture content, in the working fluid entering the gas turbine are significantly reduced. Based on the thermodynamic calculations, the only meaningful amounts of impurities present in the O_2/methane-fired sCO_2 open cycle at the turbine inlet are O_2 and H_2O, which are approximately 3.6 and 5.3 mol%, respectively. These impurity concentrations are similar to those shown in Table 2 determined from a simple mass balance.

For the O_2/syngas-fired sCO_2 open cycle, meaningful amounts of HCl and SO_2 also exist in the working fluid as impurities at the turbine inlet along with O_2 and H_2O. The HCl and SO_2 concentrations were calculated to be approximately 100 and 1000 ppm in sCO_2, respectively. A SO_2 concentration of 1000 ppm from the thermodynamic calculations is identical to that shown in Table 2 from the mass balance. However, a much higher concentration of HCl was calculated for the syngas-fired open cycle than that in Table 2.

In early commercialization of the sCO_2 open power cycle, a semi-open O_2/NG (methane)-fired system is likely the most economical and attractive. As demonstrated by the thermodynamic calculations above, the resulting sCO_2 working fluid from firing methane exhibits a minimum corrosion potential, thus allowing lower cost materials to be used. ***Consequently, the impact of O_2 and H_2O as impurities produced from an open O_2/NG-fired sCO_2 power cycle on corrosion was the focus of materials evaluation for this laboratory study.*** For closed Brayton cycles, pure sCO_2 was employed in the laboratory study as the working fluid.

EXPERIMENTAL PROCEDURES

A high-temperature, high-pressure corrosion test chamber and flow loop has been modified to perform the sCO_2 corrosion exposures at the pressure and temperature of 200 bar and 700°C, respectively. A schematic diagram of the test system is shown in Figure 1, where the major components consisted of a custom-built alloy reaction chamber, a high-pressure pneumatic-powered gas booster pump, a water injection pump, and a furnace. The test facility was housed in a secure laboratory space equipped with properly-sized exhaust, CO_2 sensor and

building monitor (in the event of a rapid CO_2 release), a private entrance door, and a video camera. A computer-based interface was installed to control the testing apparatus. All temperature and pressure sensors for the test facility were connected to a computerized data acquisition system.

The temperature profile of the pressure chamber was measured in atmospheric air at a set point of 760°C, and the results are shown in Figure 2. The isothermal working zone of the furnace at this temperature was approximately 14 inches long, and the temperature variation was less than +/-5.5°C (9.9°F). It is expected that, at the test temperature of 700°C employed for this study, the isothermal zone would have been greater than 14 inches.

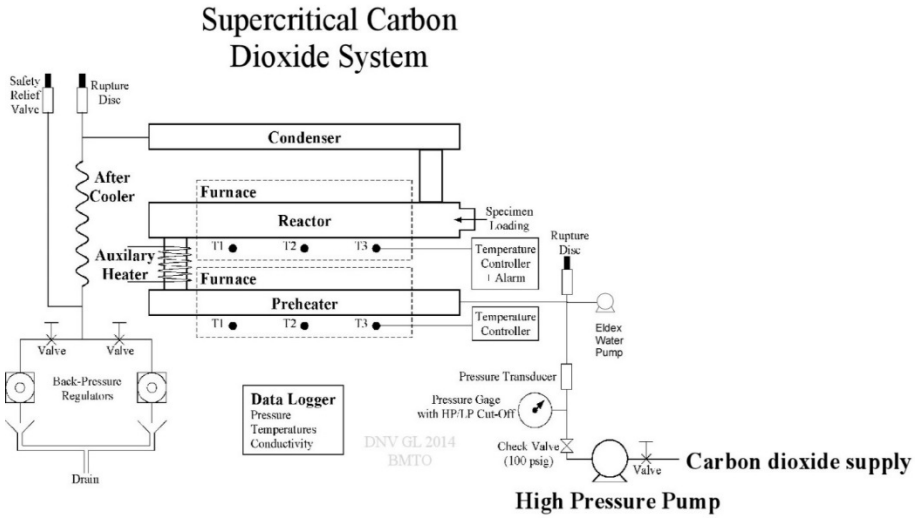

Figure 1 – Schematic diagram of the high-temperature high-pressure sCO_2 test system.

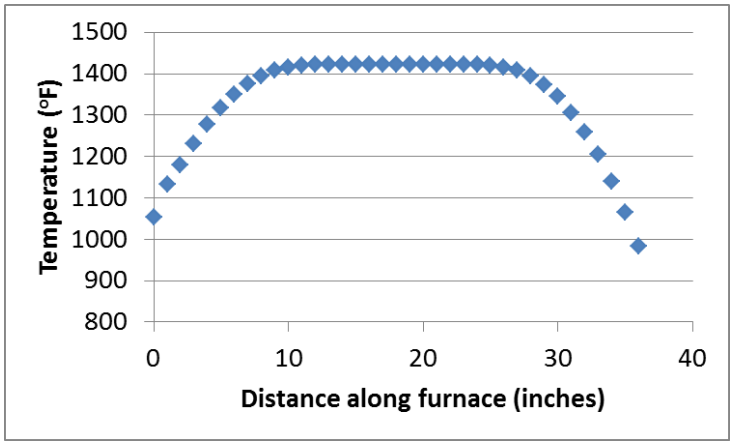

Figure 2 - Temperature profile of sCO_2 test chamber at 760°C set point.

Alloy coupons were placed in a sample holder and inserted into the working zone using a pre-measured insertion rod to ensure proper and consistent positioning inside the retort. A

Teflon gasket was installed on the threaded retort end plug, followed by the plug being torqued to approximately 50 ft-lbs. The reaction chamber was then flushed with Grade 4.8 (99.998%) nitrogen gas. The pressure barriers were checked for integrity at 200 bar under high pressure nitrogen at room temperature. Next, the reaction chamber was depressurized and flushed with the test gas at approximately 1 SLMP for 30 minutes. During the flush period, a bump test was also performed on virtual controls (i.e. open and close the solenoid valves). Subsequently, the reaction chamber was fully isolated and pressurized to approximately 35 bar using the test gas. If applicable, water was injected to the system using a calibrated Eldex high pressure piston pump. The furnace was then turned on and the working zone was heated to the desired temperature. The system pressure was risen naturally to the equilibrium pressure of about 150 bar. A high pressure gas booster pump (a Haskel pneumatic-driven gas booster pump capable of up to 5,000 psig outlet pressure) was used to increase the total system pressure to the desired pressure.

During testing, refreshing of the system was accomplished by releasing approximately twenty percent of the test pressure from the reaction chamber and replenishing the system with fresh sCO_2 using the booster pump. Steam was injected as necessary to compensate for losses during a pressure decrease. After each test, the furnace was slowly cooled to 200°C overnight and the retort was depressurized. The exposed samples were removed from the reaction chamber while warm to minimize condensation of the moisture in the test gas on the samples. All coupons were stored in a desiccator prior to weight and thickness measurements as well as metallographic preparations.

A shakedown test under the conditions of commercial-grade pure sCO_2 was performed at 700°C and 200 bar for approximately 300 hours. These test conditions would represent the environments of closed sCO_2 Brayton cycles. One inch square by 0.125 inch thick coupons of three alloys were evaluated in this test, which included ferritic steel Grade 91 (UNS K90901), austenitic stainless steel 304H (UNS S30403H), and a Ni-base alloy 740H (UNS N07740). The actual compositions of these alloys were analyzed and are summarized in Table 4. Triplicate samples for each alloy were included in this test. Measurements of the mass changes and oxide thicknesses were made on the specimens by documenting their conditions before and after the shakedown test. Results of the shakedown test demonstrated that the test facility performed satisfactorily for the intended sCO_2 laboratory study under high temperatures and pressures. The results of this 300-hour shakedown test are discussed in the next section.

Table 4
Actual compositions of alloys evaluated in laboratory tests (wt.%)

	Fe	Ni	Cr	Al	Si	Mn	Mo	V	Nb	Ti	W	N	Co	Cu	C	S
Gr 91	bal	0.12	8.38	0.011	0.3	0.44	0.93	0.2	0.063	0.003	0.16	0.047	0.02	0.09	0.1	0.001
304H	bal	8.58	18.30	<0.01	0.31	1.76	0.25	0.07	0.02	<0.01	0.02	0.06	0.15	0.36	0.07	0.005
740H	0.11	bal	24.67	1.352	0.14	0.24	0.29	0.01	1.489	1.335	0.002	0.004	20.1	<0.002	0.02	0.001

Following the shakedown test, a second 300-hour laboratory test was also performed at 700°C and 200 bar to evaluate the same alloys of Grade 91, TP304H, and 740H under a modified test condition, in which controlled levels of impurities consisting of 3.6 vol% O_2 and 5.3 vol% H_2O, were added to the sCO_2 stream. As described previously, the concentrations of these impurities were determined from mass balance and thermodynamic calculations based on an open sCO_2 Brayton cycle system. While minor amounts of sulfur and chlorine species would also present in sCO_2 depending on the fuel burned, these impurities were not considered in this study because they would not exist in sufficient quantity in an oxy/natural gas-fired sCO_2 Brayton cycle to cause significant corrosion concerns. However, the authors suggest that the impact of sulfur and chlorine from burning syngas on sCO_2 corrosion should be investigated in future research.

RESULTS AND DISCUSSION

The unit weight gains of Grade 91, 304H, and 740H coupons exposed to the pure sCO_2 in the 300-hour shakedown test at 700°C and 200 bar were determined, and the results are summarized in Table 5. Individual weight gains of the triplicate samples for each alloy along with their average value are presented. The values of the weight gains for Grade 91 are in good agreement with the results of a 500-hour laboratory study on the same alloy reported by Pint and Keiser.[5]

Table 5
Weight gains of alloy samples after exposure to commercial-grade pure sCO_2 at 700°C and 200 bar for 300 hours

Alloy	Sample #	Unit weight gain
		mg/cm²
Gr91	1	7.66
	2	8.82
	3	7.63
	Average	**8.04**
304H	1	0.28
	2	0.17
	3	0.24
	Average	**0.23**
740	1	0.19
	2	0.21
	3	0.23
	Average	**0.21**

Metallographic examinations of a representative Grade 91 sample after 300 hours of exposure to pure sCO_2 were carried out. A duplex oxide scale was evident on the surface of the sample, as shown in Figure 3, where the optical micrographs were taken at two magnifications after etching the surface with a Kallings solution. There is a dark etched band at the alloy surface adjacent to the oxide scale, which resembles carburization. The circular features away from the edge of the surface are polishing artifacts.

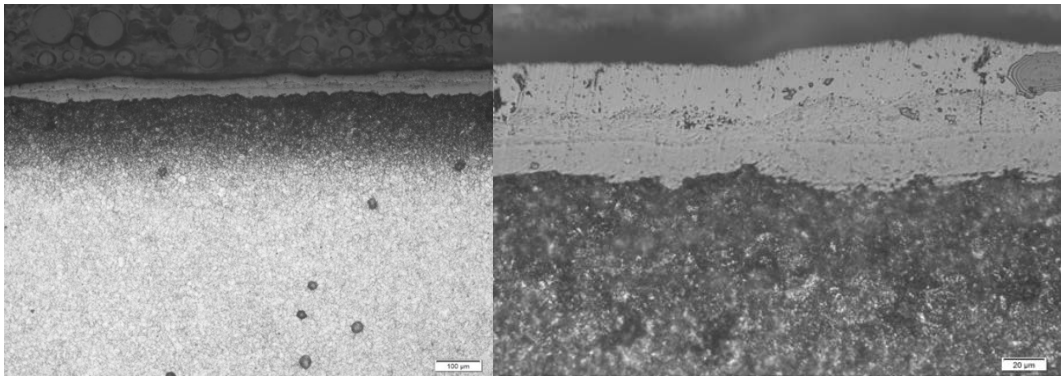

Figure 3 - Optical micrographs of Grade 91 cross-section after exposure to pure sCO_2 at 700°C and 200 bar for 300 hours.

To determine the potential of carburization for Gr 91 exposed to pure sCO_2 under the high-temperature and pressure conditions, detailed micro-hardness measurements were performed on the polished sample surface. An array of micro-hardness measurements was taken at the surface using a 100-g indenter. The indentations were approximately 60 µm apart in both directions. Figure 4 shows an optical micrograph of the finished surface after the micro-hardness measurements. Note that the first row of the measurements (shown with a horizontal red line) was taken at about 60 µm from the metal/scale interface so that any interference from the oxide was avoided.

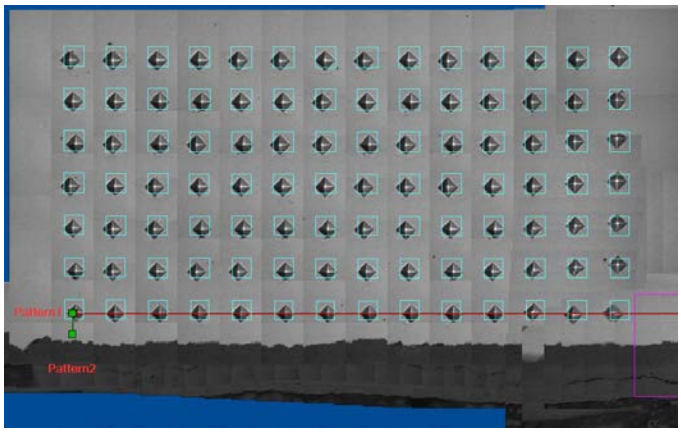

Figure 4 – Optical micrograph of a polished surface after micro-hardness measurements performed.

The measured micro-hardness data revealed hardness variations on the alloy surfaces. Figure 5 is a hardness map for Gr 91 after exposure to pure sCO_2 at 200 bar and 700°C for 300 hours, where the sample orientation correspond to that in Figure 4. From the hardness map, it is clear that the hardness at the Gr 91 surface adjacent to the scale was the highest and decreased with increasing distance from the surface. The existence of such a hardness profile is a strong evidence for carburization that had occurred on Gr 91 when exposed to pure sCO_2 during the 300-hour shakedown test

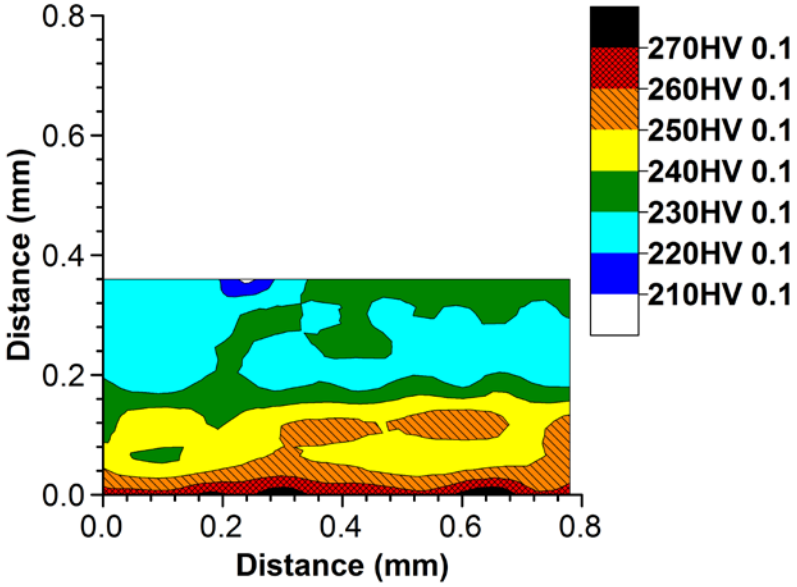

Figure 5 – Hardness map of Gr 91 showing increased hardness near the surface from carburization.

The polished Grade 91 surface was also examined using a scanning electron microscopy (SEM) equipped with energy dispersive spectroscopy (EDS). Figure 6 shows a cross-sectional SEM back-scattered electron (BSE) micrograph at the surface of the Grade 91 sample. Morphology of the oxide scale formed on the Grade 91 after exposure to sCO_2 for 300 hours appears to consist of a dual-layered structure, similar to those formed in high-temperature steam. Because carbon cannot be detected by SEM/EDS employed in this study, the dark etched band in the metal beneath the scale could not be revealed.

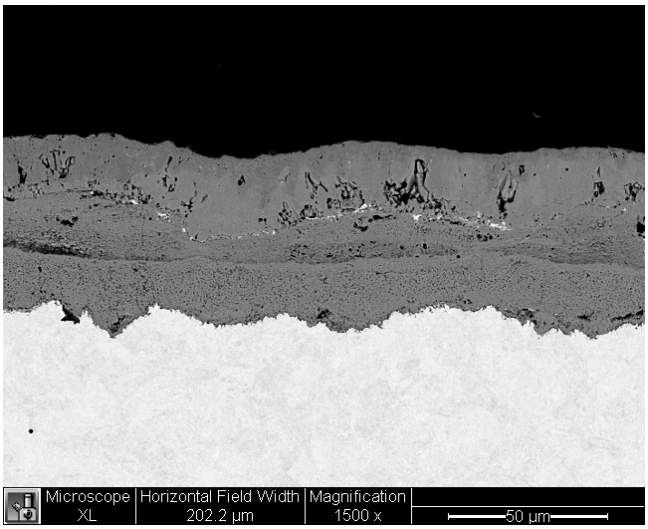

Figure 6 - Cross-sectional backscattered SEM micrograph of Gr 91 after Exposure to sCO_2 at 700°C and 200 bar for 300 hours.

EDS mapping of the key elements present on the cross-section of Gr 91 was also performed, as shown in Figure 7. Clearly, the oxide scale comprised a multi-layered structure, with an outer (magnetite) layer essentially free of Cr and an inner (spinel) layer rich in Cr. In addition, there appears to be an intermediate scale layer separating the outer and inner oxides, which consisted of two sub-layers, with the Cr concentration higher in the outer than inner. The presence of a distinct intermediate layer has not been observed on Grade 91 exposed to high-temperature steam, especially only after 300 hours. It should be pointed out that the 300-hour shakedown test experienced a pressure cycle approximately 24 hours after the start of the test. This sudden pressure drop and subsequent recovery might have contributed to the unique scale morphology. Further investigation to better understand the cause of such a scale morphology, whether unique to sCO_2 corrosion or associated with sudden pressure cycling, is warranted.

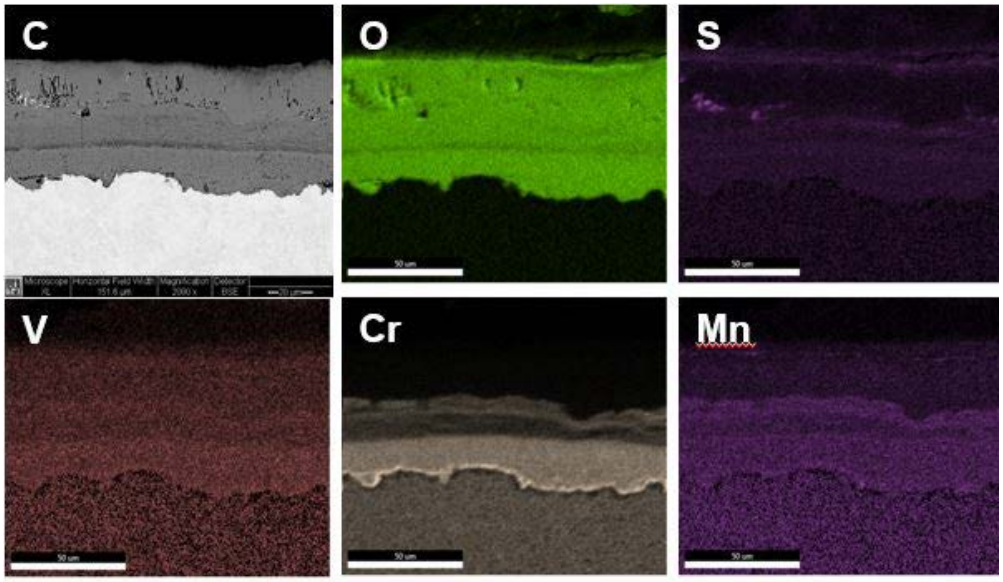

Figure 7 - Elemental Mapping of different elements for Gr 91 after exposure to pure sCO_2 at 700°C and 200 bar for 300 hours.

The results of an EDS line scan for Grade 91 are shown in Figure 8 revealing the concentration profiles of O, Cr, and Fe. The scan started within the alloy (at distance zero) and extended outward to the edge of the scale surface. Judging by the concentration profiles of these elements, a multi-layered oxide morphology with two distinct Cr-containing inner layers appears to be evident, consistent with the scale morphology shown in Figures 6 and 7.

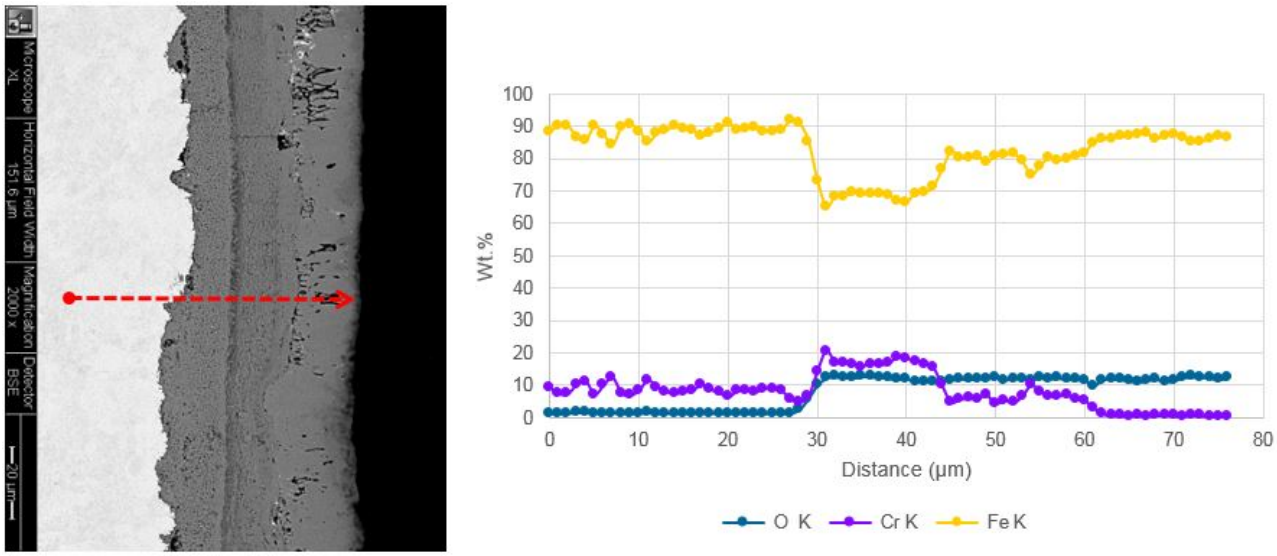

Figure 8 - EDS Line scan of Gr 91 cross-section for O, Cr, and Fe after exposure to pure sCO_2 at 700°C and 200 bar for 300 hours.

In comparison, 304H and 740H formed relatively thin oxide scales at the surfaces after exposure to the shakedown test conditions involving pure sCO_2 at 700°C and 200 bar for 300 hours. The optical micrographs of these etched cross sections for 304H and 740H in Figures 9 and 10, respectively, did not reveal a carburization band at the alloy surfaces. However, a different etchant might be required to reveal carburization for these alloys.

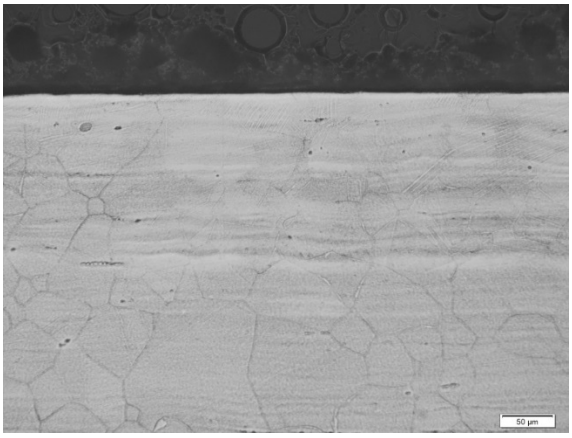

Figure 9 - Optical micrograph of 304H after exposure to pure sCO_2 at 700°C and 200 bar for 300 hours (etched with Kallings solution).

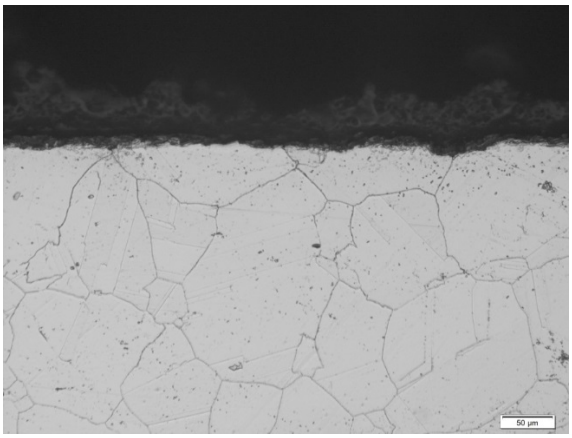

Figure 10 - Optical micrograph of 740H after exposure to pure sCO2 at 700°C and 200 bar for 300 hours (etched with Kallings solution).

The results generated from the 300-hours shakedown test under pure sCO_2 at 700°C and 200 bar, a condition representative of indirect-fired closed sCO_2 Brayton cycles, suggest that carburization can take place rapidly on the creep-strength enhanced ferritic alloy of Gr 91. Because of its relatively high Cr content in this alloy class, a similar carburization attack would be expected for all low-alloy ferritic steels that contain less Cr when exposed to high-temperature high-pressure sCO_2 environments.

Results of the second 300-hour laboratory test in sCO_2 containing 3.6% O_2 and 5.3% H_2O as impurities also showed scale formation and weight gain for the three alloys investigated. The average weight gain on the triplicate samples for each alloy is shown in Table 6. These average weight gains are consistently lower than those exposed to pure sCO_2 shown in Table 5. The lower weigh gains may be attributed to the higher oxygen partial pressure in the second test, which had promoted the formation of more protective oxide scales. Consequently, less tendency for carburization would have been experienced.

Table 6
Average weight gains of alloys exposed to impure sCO_2 containing 3.6vol% oxygen and 5.3vol% water at 700°C and 200 bar for 300 hours

Alloy	Unit Weight Gain (mg/cm^2)
Gr 91	2.79
304H	0.07
740H	0.07

Like pure sCO_2, Gr 91 formed a duplex oxide scale in the impure sCO_2 conditions, as shown in the cross-sectional SEM micrograph of Figure 11. This scale morphology is quite similar to those of Gr 91 exposed to high-temperature steam. EDS map overlay of three primary elements in the scale (i.e., iron, chromium, and oxygen) were also generated, as shown in Figure 12. The distribution of these elements confirmed a duplex scale formed on this alloy, which consisted of a magnetite outer layer and chromium-rich spinel inner layer. No intermediate layer was evident.

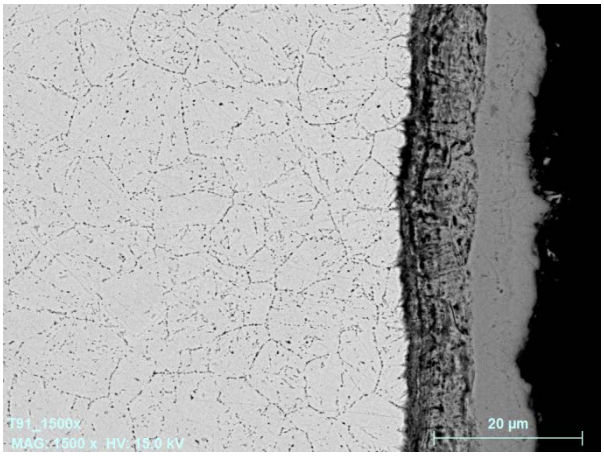

Figure 11 - Cross-sectional SEM micrograph for Gr 91 after exposure to impure sCO_2 containing 3.6vol% oxygen and 5.6vol% water at 700°C and 200 bar for 300 hours.

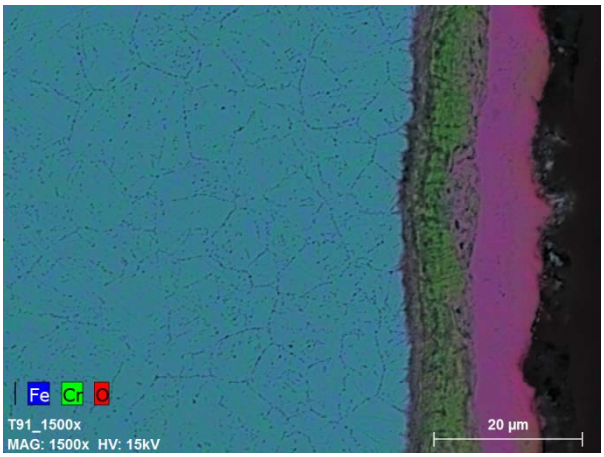

Figure 12 - EDS map overlay for Gr 91 after exposure to impure sCO2 containing 3.6vol% oxygen and 5.6vol% water at 700°C and 200 bar for 300 hours.

Extensive micro-hardness measurements and mapping were performed on this set of polished samples after exposure to the second sCO_2 test conditions containing oxygen and water as impurities at 200 bar and 700°C for 300 hours. A micro-hardness map for Gr 91 is shown in Figure 13, which clearly exhibits higher hardness values only confined to the region close to the metal surface (approximately 20 µm in depth) adjacent to the oxide scale. Beyond this region, the hardness drops off quickly to the level of the base metal. Such results suggest that carburization also occurred on Gr 91 under the impure sCO_2 test conditions, although the depth of carburization (and thus the amount of carbon pickup) was significantly less than that in Figure 5 for Gr 91 exposed to the shakedown test without impurities.

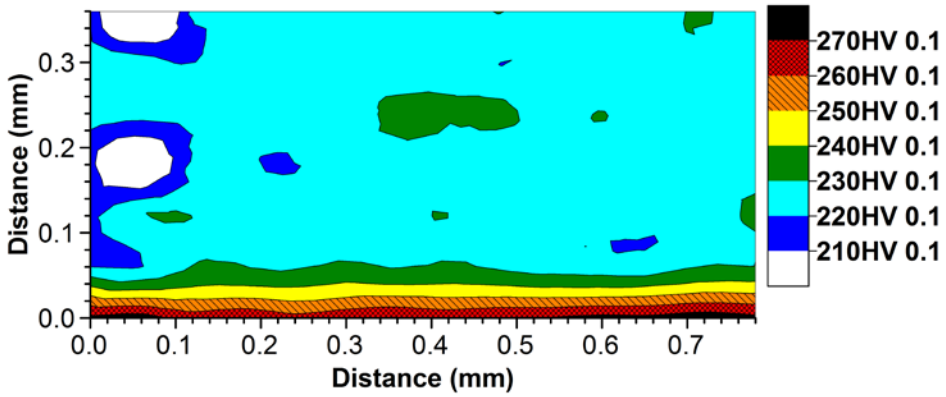

Figure 13 – Micro-hardness map for Gr 91 after exposure to impure sCO_2 containing 3.6vol% oxygen and 5.3vol% water at 200 bar and 700°C for 300 hours.

Both sets of micro-hardness maps presented in Figures 5 and 13 for Gr 91 were re-plotted against the distance from the sample surface, as shown in Figure 14. At each depth location, the entire row of 14 hardness measurements, as illustrated in Figure 4, were analyzed statistically, and the data scattering and mean value were determined and indicated in the plot. Two sets of micro-hardness maps were taken on the Gr 91 samples after exposure to the

shakedown test in pure sCO_2, which helped verify the repeatability and sensitivity of the micro-hardness measurements. Comparison of the hardness profiles for Gr 91 in Figure 14 again confirmed relatively severe carburization under the condition of pure sCO_2, up to a distance of approximately 200 µm from the metal surface, whereas carburization was confined only to the surface region under impure sCO_2, i.e., <<60 µm. Again, the less tendency for carburization in the second 300-hour test was primarily attributed to the presence of 3.6vol% oxygen in sCO_2 as an impurity, leading to the formation of more protective oxide scales.

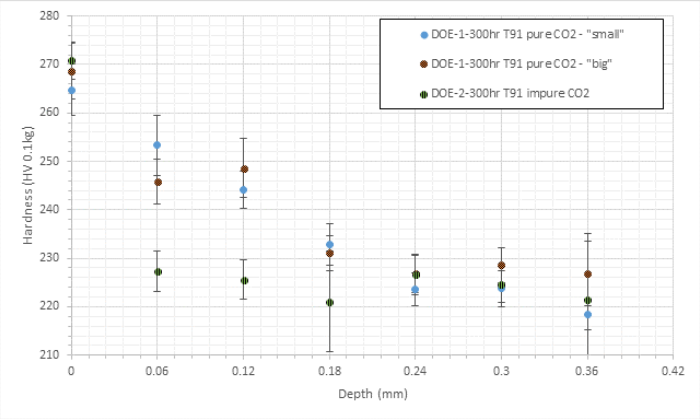

Figure 14 – Micro-hardness profiles of Gr 91 after exposures to pure and impure sCO_2 containing 3.6vol% oxygen and 5.3vol% water at 200 bar and 700°C for 300 hours.

The formation of oxide scales on 304H and 740H was negligible after the 300-hour exposure to sCO_2 containing 3.6vol% O_2 and 5.3vol% H_2O at 700°C and 200 bar. Figure 15 shows a cross-sectional SEM micrograph of the exposed 304H surface. A very thin oxide scale, approximately 2 µm, was found on the sample surface. However, an early-stage localized oxidation along the grain boundaries near the alloy surface has occurred. The yellow box and locations marked in green in this micrograph denote points where EDS analyses were performed. The EDS results revealed a chromium content of about 20wt% near the alloy surface and grain boundaries, indicating that chromium was not depleted from oxidation during the relatively short laboratory exposure. Similar thin oxides formed on 740H were also found.

Figure 15 - Cross-sectional SEM micrograph of 304H after exposure to sCO_2 containing 3.6% oxygen and 5.3% water at 200 bar and 700°C for 300 hours.

Figures 16 and 17 show the micro-hardness maps generated from the polished surfaces of 304H and 740H after exposure to the second 300-hour laboratory test conditions containing 3.6vol% O_2 and 5.3vol% H_2O as impurities. Clearly, carburization has taken place on the surface of 304H, as evident in Figure 16 by the color bands. In fact, compared to Figure 13, the depth of carburization appears to be greater in 304H than Gr 91. Such a difference is likely attributed to the difference in crystalline structure, in which the solubility of carbon is higher in austenitic 304H than ferritic Gr 91 despite the higher Cr content in the former. Because carburization had taken place on 304H during the second 300-hour test that contained a higher oxygen partial pressure, it is reasonable to assume that more severe carburization had occurred in 304H from pure sCO_2 in the 300-hour shakedown test, even though a carburized band is not revealed in Figure 9.

On the other hand, no evidence of carburization could be found in Figure 17 for 740H after exposure to the 300-hour laboratory test conditions containing impurities. The superior carburization resistance of 740H is expected because of its higher Cr and Ni contents; both elements are known to resist carburization.

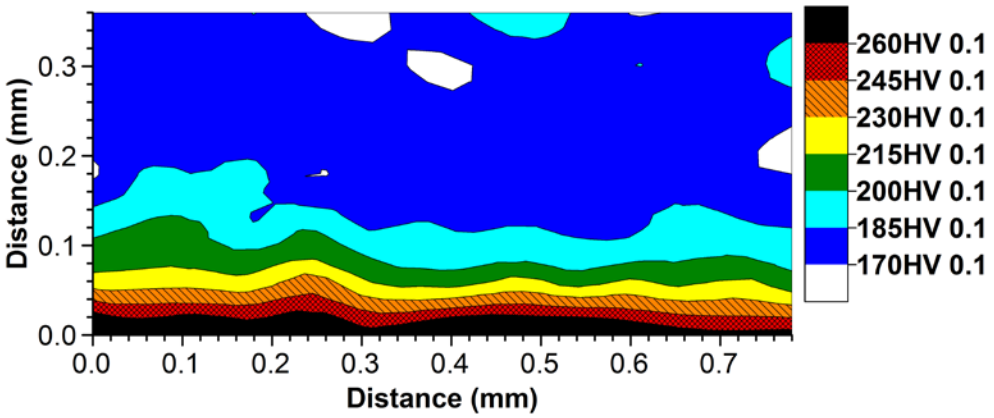

Figure 16 – Micro-hardness map for 304H after exposure to impure sCO_2 containing 3.6% oxygen and 5.3% water at 200 bar and 700°C for 300 hours.

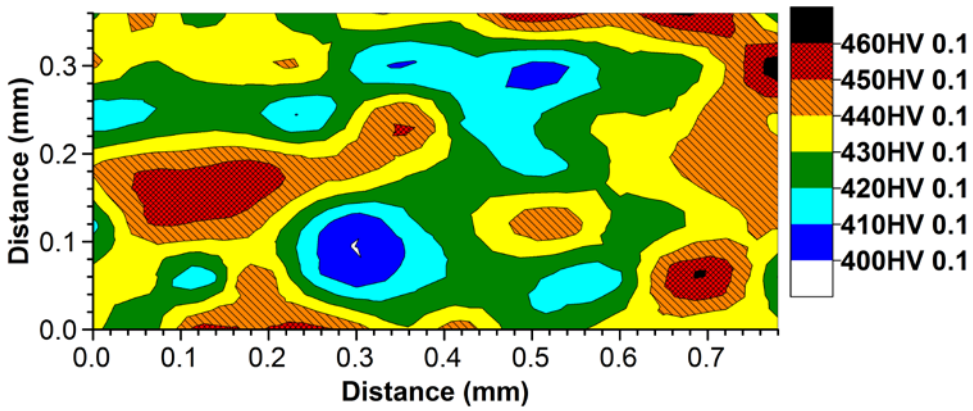

Figure 17 – Micro-hardness map for 740H after exposure to impure sCO_2 containing 3.6% oxygen and 5.3% water at 200 bar and 700°C for 300 hours.

CONCLUSIONS

A laboratory study is being performed as part of a concerted effort to generate corrosion data needed for the design and construction of key components in advanced sCO_2 Brayton power cycles. Short-term tests were conducted in the laboratory by exposing commercial alloys that are considered candidates for these applications. The laboratory tests employed sCO_2 working fluid at 700°C and 200 bar to simulate the most challenging conditions anticipated in the advanced power cycles. A detailed analysis of potential impurities using both mass balance and thermodynamic approaches was evaluated for a natural gas fired semi-open sCO2 cycle to determine the impurity concentrations for the testing. At 700°C, a thick oxide scale formed on Gr 91 after 300 hours, resulting in relatively large weight gains on the samples. On the other hand, the oxide scales formed on 304H and 740H were thin under the same test conditions, leading to little weight gains. In comparison, the weight gains of all three alloys were greater from the pure sCO_2 test at 700°C and 200 bar than those from the impure sCO_2 test containing 3.6vol% O_2 and 5.3vol% H_2O. The lower weigh gains in the impure sCO_2 test on Gr. 91 may be attributed to the higher oxygen partial pressure employed, which had promoted the formation of more protective oxide scales and consequently, less tendency for carburization been experienced. However, longer-term test data will help determine if this effect is broadly applicable to all alloys. In addition, the scale morphology formed on Gr 91 after exposure to pure sCO_2 appears to contain an intermediate layer between the magnetite and spinel oxides, which is not typically observed in high-temperature steam conditions. Such a scale morphology should be further understood and investigated. On the other hand, the scale morphology formed on Gr 91 after exposure to sCO_2 containing O_2 and H_2O as impurities did not appear to exhibit an intermediate scale layer.

Micro-hardness measurements were performed to determine the extent of carburization attack in the alloys after exposure to sCO_2 at 700°C and 200 bar. The results revealed that Gr 91 suffered severe carburization under the pure sCO_2 test conditions, with a

carburization depth up to 200 µm after only 300 hours of exposure. Less carburization was observed in Gr 91 when exposed to impure sCO_2 containing O_2 and H_2O. The less tendency for carburization in the impure sCO_2 may be attributed primarily to the higher partial pressure of oxygen, resulting in the formation of more protective oxide scales. Carburization was also found in 304H after exposure to the impure sCO_2 under the test conditions for 300 hours. In fact, under the same test conditions, more severe carburization occurred in 304H than Gr 91, possibly due to the austenitic crystalline structure and thus a higher carbon solubility. On the other hand, no evidence of carburization was found in 740H. The superior carburization resistance of 740H is expected because of its higher Cr content as well as being a nickel-base alloy. Both of these elements have been known to resist carburization.

Based on this testing, a longer-term laboratory test program has started on a wider array of alloys using the impure sCO_2 for multiple temperatures and times up to 1,000 hours to develop oxide scale growth kinetics in support of a robust model for long-term component prediction.

ACKNOWNLEDGEMENTS

The authors would like to acknowledge the funding support of the U.S. Department of Energy under Contract No. DE-FE0024120 (Project Manager: Vito Cedro III). Special thanks to Trent Almond, EPRI, for his assistance with microhardness mapping.

REFERENCES

1. System and Method for High Efficiency Power Generation using a Carbon Dioxide Circulating Working Fluid. US Patent 2011/0179799 A1, July 28, 2011.
2. R.J. Allam, M. R. Palmer, G. W. Brown Jr, J. Fetvedt, D. Freed, H. Nomoto, M. Itoh, N. Okita, and Charles Jones, High Efficiency and Low Cost of Electricity Generation from Fossil Fuels while Eliminating Atmospheric Emissions, Including Carbon Dioxide, Energy Procedia 37 (2013) 1135–1149.
3. Cost and Performance for Fossil Energy Plants Volume 1: Bituminous Coal and Natural Gas to Electricity, Revision 2a, DOE/NETL-2010/1397, September 2013.
4. A Roine, HSC Chemistry 8.0, Outotec, August 29, 2014.
5. B.A. Pint and J.R. Keiser, 'The effect of temperature on the sCO2 compatibility of conventional structural alloys,' Paper no. 61 presented at the *4th International Symposium - Supercritical CO_2 Power Cycles*, September 9-10, 2014, Pittsburgh, Pennsylvania.